ARTICLE

Multidisciplinary study on the hydrogelation of digold(I) complex [{Au(^{9}*N*-adeninate)}$_2$(μ-dmpe)]: optical, rheological, and quasi-elastic neutron scattering perspectives

Received 00th January 20xx,
Accepted 00th January 20xx

DOI: 10.1039/x0xx00000x

Daniel Blasco,[a] José M. López-de-Luzuriaga,*[a] Miguel Monge,[a] M. Elena Olmos,[a] María Rodríguez-Castillo,[a] Hippolyte Amaveda,[b] Mario Mora,[b] Victoria García Sakai[c] and José A. Martínez-González.[c]

Herein, the syntheses of [{Au(^{9}*N*-adeninate)}$_2$(μ-dmpe)] (**2**, dmpe = 1,2-bis(dimethylphosphino)ethane) and its chloride precursor [(AuCl)$_2$(μ-dmpe)] (**1**) are described. X-ray diffraction of **2** reveals a short intramolecular aurophilic interaction (2.9919(8) Å), which is present even when **2** crystallizes from its own hydrometallogel (3.0512(3) Å). This interaction is demonstrated by TD-DFT calculations to be participant in the intense blue phosphorescence that **2** displays in the solid state and, presumably, also in the hydrogel one. Finally, as complex **2** could be understood as a formal dimer of LMWG [Au(^{9}*N*-adeninate)(PMe$_3$)] (**3**), the hydrogelation of the former is examined, with special regard to its optical, rheological and quasi-elastic neutron scattering properties, which are compared to those of **3**.

Introduction

Among transition metal complexes, gold(I) coordination and organometallic ones are of great interest in their application as Low-Molecular-Weight Gelators (LMWGs).[1-4] In fact, the tendency of closed-shell late transition metals to be disposed at distances lower than the sum of their van der Waals radii, which is maximum for gold(I) due to its high relativistic effects (the so-called aurophilicity phenomenon),[4,5] is a contributing force, if not the pivotal one, for the self-assembly of such molecules in solution. This usually renders long nanofibers which act as a solvent trap, due to dense entanglement, giving rise to the continuous gel texture that is macroscopically identified by testing its resistance to the inversion of the container.[6]

Since the seminal structural works and modelling calculations that were published as early as in the 1980's, the aurophilicity concept has reached scientific maturity revealing that, not being an exclusive phenomenon of gold(I), the more general concept of metallophilicity is indeed, an "unexpected" London-type attraction between electron-rich metals. Therefore, it should be noted that aurophilicity (or metallophilicity) is not a crystal structure-imposed result, but an inherent self-assembly capacity of gold(I) which happens when the global energetics are favorable towards its formation, taking into account that the stabilization effect (30-50 kJ·mol^{-1}) is comparable to that of moderate hydrogen bonding.[7] Such competition between weak forces comes to be particularly true for fluid phases as gels, for which the *a priori* design of functional gold(I) "aurophilic" gelators is still unreachable. Despite that, aurophilicity is dramatically favored and strengthened using ditopic ligands with short spacers, which force their digold(I) complexes to display sub-van der Waals Au^I···Au^I distances. In those cases, that ligand-supported aurophilic interaction is a common source of phosphorescence, resulting from the deactivation of the Au^I···Au^I centered ^{3}($d\sigma^*p\sigma$) or ^{3}($d\delta^*p\sigma$) excited states, if no lower energy ligand-based orbitals participate in the possible emission.[8-10] The luminescent emission is also enhanced by the reduction of energy dissipation by molecular motions (rotation, vibration or translation) due to the increased rigidity of the bridging ligand.[11]

Our own strategy for the development of new gold(I)-based LMWGs relies in the application of the isolobal analogy between cationic [Au(PMe$_3$)]$^+$ units and H$^+$ itself,[12,13] aiming to obtain new materials which combine the hydrogen bonding pattern of the ligand of choice with the attractive features displayed by gold(I), which, apart from aurophilicity, also include the still discussed possibility of acting as a hydrogen bond acceptor (X-H···Au^I; X = C, N, O; E_{int} < 17 kJ·mol^{-1}).[14] Thus, the substitution of the acidic proton of nucleobase adenine (**Chart 1**, left) by [Au(PMe$_3$)]$^+$ leads to the formation of LMWG [Au(^{9}*N*-adeninate)(PMe$_3$)] (**Chart 1**, center-left), which, in fact, forms a blue-luminescent hydrogel at a concentration of 100 mg·mL^{-1}.[15] The origin of its luminescence has been attributed to the establishment of Au^I···Au^I interactions in the gel state; also, we have found that dimerization through aurophilicity is the first step in the formation of the hydrogel. On the other side, the coordination of [Au(PMe$_3$)]$^+$ (as its trifluoroacetate complex) to

[a] *Departamento de Química, Centro de Investigación en Síntesis Química (CISQ), Universidad de La Rioja, Madre de Dios 53, 26004 Logroño (Spain).*
[b] *Instituto de Nanociencia y Materiales de Aragón, INMA (CSIC-Universidad de Zaragoza), María de Luna 3, 50018 Zaragoza (Spain).*
[c] *ISIS Neutron and Muon Source, Rutherford Appleton Laboratory (RAL), Harwell Science and Innovation Campus, OX11 0QX Chilton, Didcot (United Kingdom).*

Electronic Supplementary Information (ESI) available: instrumentation, syntheses, spectroscopic characterization, structural characterization, optical properties, computational studies, atomic coordinates of computational optimizations (*xyz* format). See DOI: 10.1039/x0xx00000x

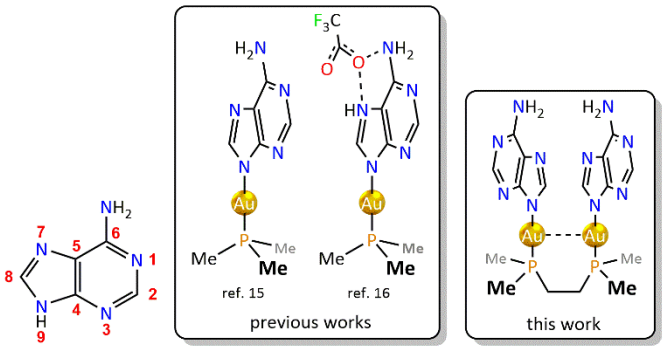

Chart 1 Canonical numbering of adenine, and molecular structures of LMWGs [Au(9*N*-adeninate)(PMe$_3$)], [Au(9*N*-adenine)(PMe$_3$)](CF$_3$CO$_2$) and [{Au(9*N*-adeninate)}$_2$(μ-dmpe)].

neutral adenine renders [Au(9*N*-adenine)(PMe$_3$)](CF$_3$CO$_2$) (**Chart 1**, center-right).[16] Despite it forming a hydrogel at lower concentrations than the former (40 mg·mL^{-1}), the absence of Au^{I}···Au^{I} interactions in the crystalline structure correlates with its non-luminescent behavior in both solid (rt) and gel states.

In view of these results, we wondered if the substitution of monodentate trimethylphosphine (PMe$_3$) in the adeninategold(I) complexes by a small α,ω-diphosphine ligand such as 1,2- bis(dimethylphosphino)ethane (dmpe) would lead to new LMWG materials with different properties. The choice of dmpe is by no means arbitrary: it can be considered as a formal dimer of PMe$_3$, making the first dimerization step through non-supported Au^{I}···Au^{I} interactions unnecessary for final aggregation up to the gel state.

Hence, the syntheses of [{Au(9*N*-adeninate)}$_2$(μ-dmpe)] (**2**) and its chloride precursor [(AuCl)$_2$(μ-dmpe)] (**1**), by straightforward methods, are herein presented. Complex **2** is fully characterized, X-ray diffraction shows two different pseudo-polymorphs, and its photoemissive properties are explained with the aid of computational methods. Finally, the hydrometallogel of **2** has been examined by two techniques which are unusual in a synthetic inorganic chemistry report: oscillatory rheology and quasi-elastic neutron scattering, focusing in the comparison between "dimeric" [{Au(9*N*-adeninate)}$_2$(μ-dmpe)] (**2**) and "monomeric" [Au(9*N*-adeninate)(PMe$_3$)] (henceforth, **3**), forms.

Results and discussion

Synthesis and characterization

Complex [(AuCl)$_2$(μ-dmpe)] (**1**) is prepared as a single batch by displacement of the labile tetrahydrotiophene (tht) ligand from [AuCl(tht)] by dmpe diphosphine, in argon-protected anhydrous tetrahydrofuran solution. Further attack of two equivalents of deprotonated adenine (as adeninate sodium salt) to **1** in refluxing absolute ethanol forms the desired [{Au(9*N*-adeninate)}$_2$(μ-dmpe)] (**2**) compound in a high yield (see **Scheme 1**).

The registered spectroscopic and physical data are consistent with the proposed stoichiometry for both compounds. In this sense, the observation of an IR absorption band at 310 cm^{-1} for **1**, assigned to ν(Au-Cl) stretching, relates to its formation. This band is not present in the IR spectrum of **2**, advancing the effective substitution of the chlorido ligand by the adeninate anion (see **Figure S3**). Turning back to **1**, the appearance of resonances from the phosphinic protons in the ^{1}H NMR spectrum and, lastly, a sharp singlet in the ^{31}P{^{1}H} NMR spectrum at 5.5 ppm, evidence the formation of one single compound with an identical coordination environment for both phosphorus atoms. With regards to complex **2**, new singlet resonances with origin in the incorporated adeninate moieties appear in the ^{1}H NMR spectrum, at 8.13 (^{2}CH) and 7.75 (^{8}CH) ppm, and in an appropriate integer ratio with respect to those of dmpe. In a similar mode to **1**, a sharp singlet at -1.2 ppm in the ^{31}P{^{1}H} NMR spectrum demonstrates the symmetric coordination of both adeninate fragments to gold(I), taking place at ^{9}N (see **X-ray crystal structure determination**). As advanced, no ν(Au-Cl) stretching absorption is observed in the low energy region of the IR spectrum of **2** and, in addition, a new broad band with maxima at 3315 and 3170 cm^{-1} appears (partially overlapped with the intense absorptions of the nujol oil and the polyethylene sample support), assigned to the stretching modes of the ^{6}C-amino group of the adeninate ligands. Finally, the ESI-MS spectra confirm the presence of adeninate (*m/z* = 134.0 Da in the negative mode) and, indirectly, the formation of **2** due to the observing of hypothetic [Au$_2$(μ-adeninate)(μ -dmpe)]$^{+}$ (*m/z* = 678.1 Da in the positive mode), as a result of the loss of one adeninate ligand.

X-ray crystal structure determination

Suitable single crystals of **2**·1.25EtOH were obtained by the slow diffusion of *n*-hexane onto an ethanolic solution of the complex. Experimental details and selected bond lengths and angles are collected in **Tables S1-S3**. The complex crystallizes in the triclinic

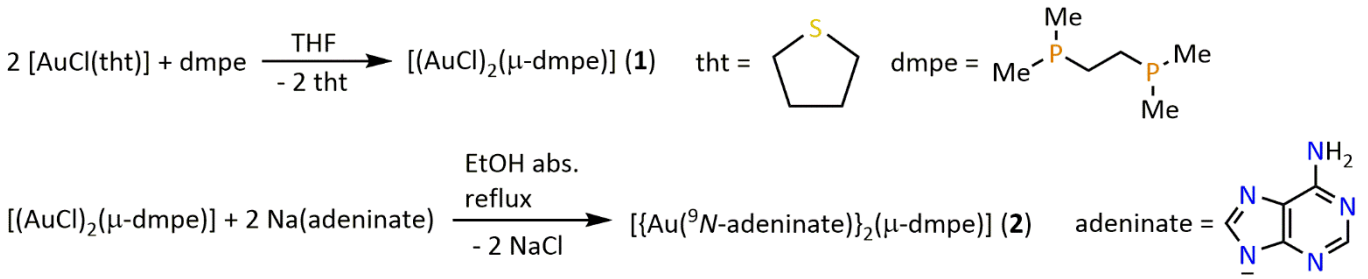

Scheme 1 Syntheses of complexes **1** and **2**.

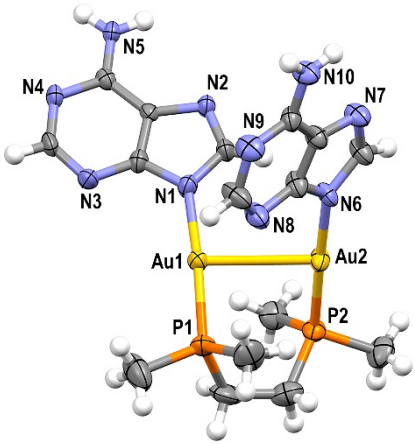

Figure 1 Asymmetric unit of the X-ray structure of **2**·1.25EtOH (40% probability ellipsoids), with the labelling scheme of the atom positions. Ethanol molecules had been omitted for clarity. Color code: C, gray; H, white; Au, yellow; N, blue; P, orange.

P-1 space group, with two formula units per unit cell, accompanied by two and a half crystallization ethanol molecules. The geometry around each gold(I) center is, as depicted in **Figure 1**, almost linear (^{9}N-Au-P angles of 175.0(4)° and 178.0(3)°), appearing the metal coordinated to one phosphorus atom of dmpe and to the ^{9}N position of the adeninate ligand, as in the other reported mono- and diphosphine analogs.[15-20] Au-P bond distances of 2.238(4) and 2.241(4) Å, and Au-N of 2.030(11) and 2.027(11) Å, are comparable to those of previously reported adeninategold(I) complexes ([Au(^{9}*N*-adeninate)(PMe_3)],[15] Au-P: 2.233(3), 2.231(3) Å; Au-N: 2.048(10), 2.043(10) Å; [Au(^{9}*N*-adenine)(PMe_3)](CF_3CO_2),[16] Au-P: 2.238(2) Å; Au-N: 2.068(7) Å; [Au(^{9}*N*-adeninate)(PEt_3)],[17] Au-P: 2.238(2); Au-N: 2.057(5) Å; [Au(^{9}*N*-adeninate)(PPh_3)],[18] Au-P: 2.240(1); Au-N: 2.038(4) Å; [Au(^{9}*N*-adeninate)(PTA)]·H_2O,[19] Au-P: 2.230(4), 2.221(2), 2.231(2) Å; Au-N 2.060(5), 2.044(5), 2.064(5) Å; [{Au(^{9}*N*-adeninate)}$_2$(μ-dppp)],[20] Au-P: 2.2347(11), 2.2361(10); Au-N: 2.040(4), 2.036(6) Å). The relative *gauche* disposition of the dimethylphosphino groups along the carbon-carbon bridge bond (P-C-C-P torsion of -63.45°, **Figure S10**) allows the appearance of a semi-supported short aurophilic interaction of 2.9921(7) Å which, in fact, is the shortest value reported to date for this type of complexes ([Au(^{9}*N*-adeninate)(PMe_3)],[15] 3.2081(6) Å; [Au(^{9}*N*-adeninate)(PTA)]·H_2O,[23] 3.2122(4), 3.2307(4), 3.2697(4) Å), but is slightly longer than those of the doubly-bridged cationic bis(μ-diphosphine)diauracycles ([Au_2(μ-dmpe)$_2$](ClO_4)$_2$·H_2O, 2.872(2) Å; [Au_2(μ-dmpe)$_2$]Cl_2·2 H_2O, 2.9265(5) Å; [Au_2(μ-dmpe)$_2$]Br_2·1.5 H_2O, 2.9438(6) Å; [Au_2(μ-dmpe)$_2$]I_2·CH_3CN, 2.974(3) Å).[21] This interaction is responsible for the bright blue phosphorescence displayed by **2** in the solid state and, probably, in the hydrogel form (*vide infra*). The measured distance between gold(I) centers of consecutive dimers along the *b* axis, of 7.492 Å, is much longer than the double of the van der Waals radius of gold(I) (2 × 1.62 Å).[22] However, a ^{2}C-H···Au^{I} hydrogen bond to gold(I) of 2.809 Å appears along the same axis, which may contribute to the overall stabilization of the structure. A similar interaction was found in the crystal structure of [Au(^{9}*N*-adenine)(PMe_3)](CF_3CO_2),[16] with an estimated strength of -12.45 kJ·mol^{-1} (MP2 level of theory), being considered as a relevant directing force in the straight nanofiber growth that is observed for that compound in water solution.

The crystalline packing of **2**·1.25EtOH resembles that of [Au(^{9}*N*-adeninate)(PMe_3)].[15] So, in **2**·1.25EtOH adeninate ligands are paired by ^{6}CN-H···^{7}N and ^{6}CN-H···^{1}N hydrogen bonds between ^{6}C-amino hydrogen atoms and the ^{7}N or ^{1}N positions of symmetry-related neighboring [{Au(^{9}*N*-adeninate)}$_2$(μ-dmpe)] molecules, and also by ^{6}CN-H···O and O-H···^{1}N hydrogen bonds with the crystallization ethanol molecules, that act as bridges between pairs of title molecules. This bonding pattern, along with the ^{2}C-H···Au^{I} hydrogen bonds, forms a folded sheet-like motif (**Figure 2**) which is stacked along the *a* crystallographic axis by a combination of weaker interactions.

Incidentally, we obtained good-quality single crystals that spontaneously grew from the hydrometallogel matrix of **2** at room temperature (*vide infra*). In this condition, the complex crystallizes again in the triclinic *P*-1 space group, with two formula units per unit cell; also, four crystallization water molecules appear. Experimental details and selected bond lengths and angles are presented in **Tables S1** and **S4-S5**. Despite the coordination environment of gold(I) here being virtually identical to that previously described for **2**·1.25EtOH (bond distances Au-P: 2.2436(15), 2.2472(15) Å; Au-^{9}N:

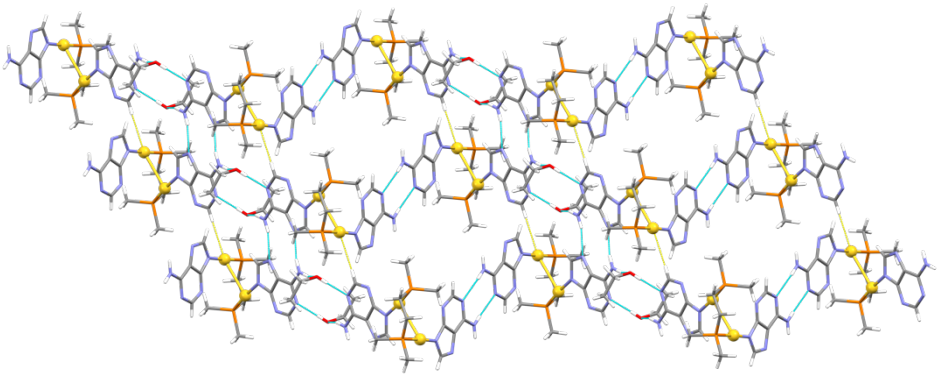

Figure 2 Bidimensional expansion of **2**·1.25EtOH through hydrogen bonds (blue dashes) and hydrogen to gold(I) contacts (yellow dashes), as seen along the *a* axis. Colour code: C, grey; H, white; Au, yellow; N, blue; O, red; P, orange.

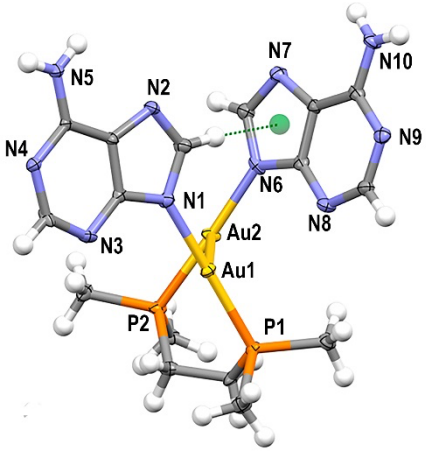

Figure 3 Asymmetric unit of the X-ray structure of **2**·2H_2O (40% probability ellipsoids), with the labelling scheme of the atom positions. Water molecules had been omitted for clarity. Color code: C, gray; H, white; Au, yellow; N, blue; P, orange; centroid, green.

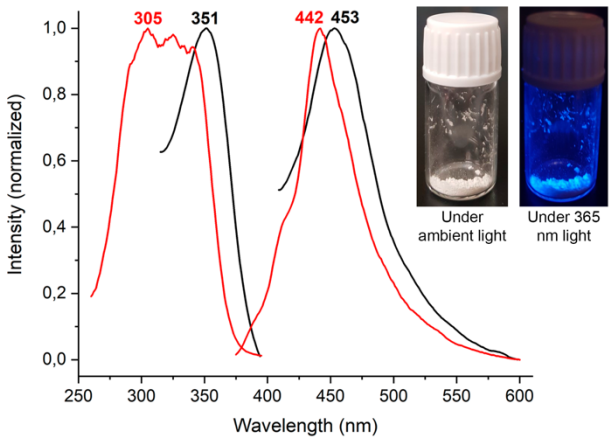

Figure 4 Excitation and emission spectra in the solid state of complex **2** at room temperature (black) and 77 K (red). Inset: photographs of solid **2** under ambient and 365 nm UV light.

2.049(5), 2.060(5) Å; bond angles ^{9}N-Au-P: 177.63(14)°, 177.27(15)°; see **Figure 3**), the bridging dmpe ligand is considerably more twisted (P-C-C-P torsion increases up to 97.51°, **Figure S10**) and, consequently, the semi-supported aurophilic interaction, albeit still present, elongates to 3.0512(3) Å. Moreover, a new C-H···π interaction of 2.529 Å, which is clearly absent in **2**·1.25EtOH, arises between ^{8}CH and the electron density of the imidazole ring of the other adeninate ligand, as depicted in **Figure 3**.

The crystalline packing of **2**·2H_2O is highly contrasting to that of the ethanol pseudo-polymorph. In fact, the presence of water molecules in the network which, in addition to being smaller provide additional points for hydrogen bonding, leads to the formation of a more compact and complex supramolecular arrangement. So, one of the two crystallographically independent water molecules that are assigned in the unit cell acts both as donor (O-H···^{1}N, O-H···^{3}N) and acceptor (^{6}CN-H···O) of hydrogen bonding, assisting the overall stabilization of the repetitive structural motif that is depicted in **Figure S11**. Apart from those, usual adeninate···adeninate ^{6}CN-H···^{7}N hydrogen bonds are also contributive.

Optical properties

The Vis-UV absorption spectrum of **2** has been recorded from a 5·10^{-5} M aqueous solution and compared to that of free adenine. As can be seen in **Figure S12**, complex **2** and its parent nucleobase show very similar profiles, with a high energy band at 204 nm and a less intense one at 251 nm, despite new transitions at 224 and 269 nm appear as shoulders in the data for the former. A previous study on the absorption of mononuclear [Au(^{9}*N*-adeninate)(PEt_3)] in water suggested that auration does not significantly perturb the π-delocalized system of adenine,[17] so intraligand $\pi \rightarrow \pi^*$ transitions are also considered here as the origin of the absorption of **2**. Similar conclusions can be extracted from the inspection of the DRUV-Vis spectra of complexes **1-2** and free adenine in KBr mulls (**Figure S13**).

The photoemissive properties of **2** in the solid state have also been examined. When the amorphous solid of complex **2** is irradiated with a UV hand lamp of 365 nm, a bright blue luminescence is observed (inset photographs in **Figure 4**). This emission appears as a non-structured band with a maximum at 453 nm (excitation at 351 nm), and an associated absolute quantum yield of 11.4%. When cooling the sample to 77 K, the emission profile blue-shifts to 442 nm and the excitation spectrum broadens as a continuum, ranging from 305 to 340 nm. The lifetime of the emission at both temperatures lies in the nano-to-microsecond range (617 ns at rt, 1397 ns at 77 K), suggesting a phosphorescent deactivation of the excited state which agrees with the large Stokes shifts of 6415 cm^{-1} (rt).

Computational studies

To gain insight into the origin of the optical and photophysical properties of **2** in the solid state, DFT and TD-DFT calculations were carried out. A [{Au(^{9}*N*-adeninate)}$_2$(μ-dmpe)]$_2$ dimer model was built from the X-ray structure of **2**·EtOH, considering two title molecules interacting by ^{6}CN-H···^{7}N hydrogen bonds, as previously explained, which was optimized at the DFT-D3/PBE level of theory constrained at the C_i symmetry group (model **2a**). A dimer model was preferred rather than a monomer one, to override the intramolecular π-stacking interaction that is established between the adeninate ligands when just a single molecule of **2** is freely optimized (check **Figure S14** for different views of the result of such optimization). The optimization of **2a** shows a nice match with the considered fragment of the X-ray network of **2**·EtOH (**Figure 5**); in particular, the calculated Au^{I}···Au^{I} distance of 2.99 Å is virtually identical to the observed one (2.9919(8) Å), thus validating both the theoretical model and the derived time-dependent properties. Further structural comparations are collected in **Table S6**.

The analysis of the electronic structure of the frontier molecular orbitals of **2a** reveals that, whereas HOMO and HOMO-1 orbitals are fully located over the hydrogen-bond interacting adeninate ligands, LUMO and LUMO+1 ones show a major, clearly bonding contribution along the Au^{I}···Au^{I} interaction axis, being the remaining ligands' contribution to the orbital subsidiary. This suggests that the LUMO (and LUMO+1) orbital

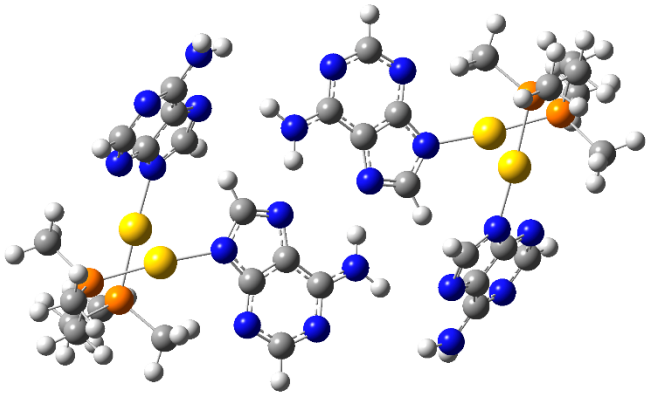

Figure 5 Representation of the theoretical model **2a**.

possesses major 6*s*/6*p* character, giving rise to a *pσ* electronic state (as in $[Au_2(\mu\text{-dppm})_2]^{+}$)[8,9], which illustrates the importance of the intramolecular aurophilic interaction in the description of the electronic structure of **2**.

Over the minimized structure of **2a**, a TD-DFT calculation of the first symmetry-allowed singlet-to-singlet transitions was performed to simulate the absorption spectrum. In accordance with the photophysical measurements, which suggest a phosphorescent phenomenon for **2** (τ = 617 ns at rt), the lowest energy singlet-to-triplet transition was also computed. Results are collected in **Table S7** and depicted in **Figure 6**, along with the DRUV-Vis absorption and excitation spectra of **2**.

This calculation suggests that the first singlet-to-triplet transition is, in fact, a mixture of two main contributions, which arise as ligand to metal···metal charge transfers (^{3}LMMCT) from both HOMO and HOMO-1 to LUMO or LUMO+1, respectively (**Figure 6**, bottom). The predicted energy of such transition, which is not included within the absorption spectrum according to its spin forbiddance, is close to the experimental excitation, although slightly red-shifted with respect to its maximum.

Hydrogelation properties

Complex [{Au(9*N*-adeninate)}$_2$(μ-dmpe)] (**2**) is, as expected from the presence of two adeninate ligands in its structure, freely soluble in water. This allowed us to prepare highly concentrated aqueous solutions of **2** just by gentle heating, which, once cooled to room temperature, started forming a transparent hydrometallogel. A photograph of the gel is included in **Figure 7** for illustrative purposes. In comparison to the previously reported [Au(9*N*-adeninate)(PMe_3)][15] gels, a smaller mass of the LMWG are needed for the preparation of a self-standing gel. Moreover, it is also formed in a shorter time.

A more exhaustive study on the determination of the critical gelation concentration (cgc) of **2** revealed that, even at a concentration of 20 mg·mL^{-1}, the complex's solutions are more viscous than neat water, although the viscosity is slowly increased upon aging, and such phases do not withstand the inversion-of-the-vial test. The cgc of **2** has been finally determined to be *ca*. 40 mg·mL^{-1}, notably lower than that of [Au(9*N*-adeninate)(PMe_3)] (100 mg·mL^{-1})[15] and similar to that of [Au(9*N*-adenine)(PMe_3)](CF_3CO_2) (40 mg·mL^{-1}).[16]

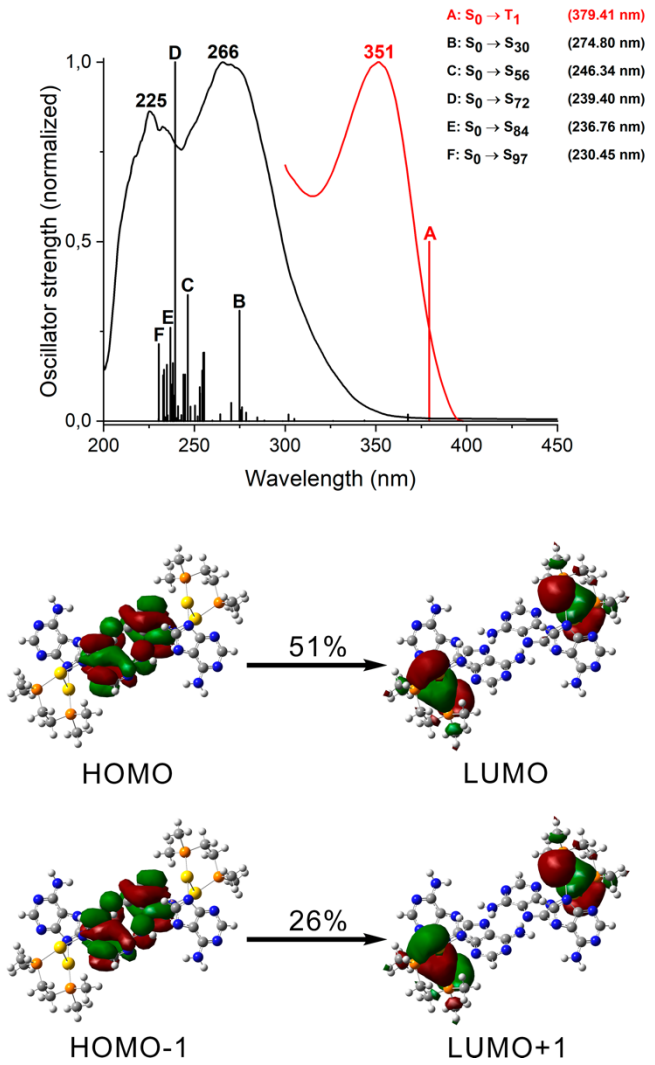

Figure 6 Top: TD-DFT singlet-to-singlet (black bars) and first singlet-to-triplet (red line) transitions of model **2a**, superimposed with DRUV-Vis (black line) and excitation (red line) spectra of complex **2**. Bottom: molecular orbitals involved in the most relevant contributions (in %) to the first singlet-to-triplet excitation.

Interestingly, when the hydrogel is prepared under oxygen exclusion conditions, it displays blue photoluminescence when irradiated with 365 nm light (**Figure 7**, right). The variation of

Figure 7 Photographs of the inversion-resistant hydrometallogel of **2** (50 mg·mL^{-1}), under ambient (left) and 365 nm UV light (right).

the emission intensity of a 50.0 mg·mL^{-1} hydrogel of **2** with increasing temperature from 30 °C to 60 °C is depicted in **Figure S16**, and a continuous decrease in the luminescence intensity upon heating is observed. This can be attributed to both thermal deactivation of the excited emissive states and the thermoreversible gel-to-sol transition that is observed along that temperature range.

The mechanical response of the hydrogel was examined by oscillatory strain and frequency sweep experiments. Those of [Au(9*N*-adeninate)(PMe$_3$)] (**3**) in its hydrogel state are also included in here for completeness and comparative purposes. Storage (*G'*) and loss (*G"*) moduli versus increasing strain values, measured at a constant frequency of 0.7958 Hz (5 rad·s^{-1}), are plotted in **Figure 8** for both complexes at the same concentration of 100 mg·mL^{-1}. It is noteworthy that quite different storage moduli and yield stress (τ^*) values are obtained for such similar complexes under identical experimental conditions. In fact, despite both behaving as proper gels in their linear regime ($G' > G''$ for $\tau < \tau^*$), the hydrogel of **3** is almost an order of magnitude more robust than that of **2**. This confirms the laboratory observation that, while simple manual shaking is enough for disrupting the hydrogel texture of **2**, especially at low concentrations, no gel-to-sol transition is apparent for **3** even when massive displacement and spattering of the material occurs.

The relative mechanical fragility of **2** may be explained by its propensity towards the crystallization of **2**·2H$_2$O from the gel network, and the peculiar nanostructure that is revealed by *cryo*-STEM (*vide infra*). Spontaneous crystallization from alkali metal-templated guanosine hydrogels is known to occur because the gel phase is, in fact, a kinetically entrapped state favoured by the fast thermodynamics of the process.[23,24] Thus, an analogous explanation may be adopted in here.

Finally, the nanoscale structure of the hydrogel has been investigated in terms of cryo-STEM microscopy of a diluted sample (1:4 in distilled water). Representative micrographs at a series of microscopic augmentations are presented in **Figure 9**, which show the curious texture of this soft material. The nanostructure of the gel is like that of a sponge, being the result

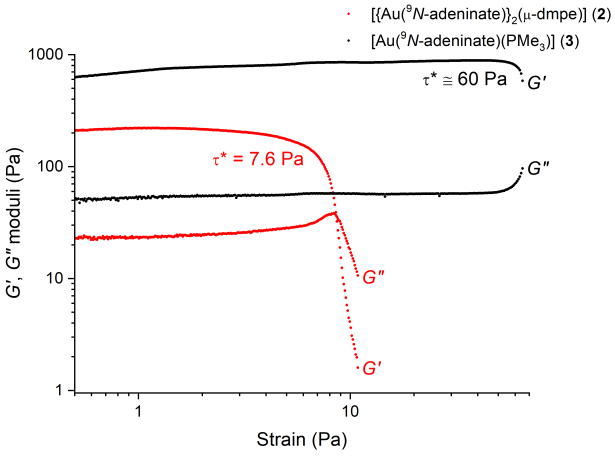

Figure 8 Strain sweep (constant frequency: 0.7958 Hz) of [Au(9*N*-adeninate)(PMe$_3$)] and [{Au(9*N*-adeninate)}$_2$(μ-dmpe)] (**2**) hydrometallogels (10% (w/w)).

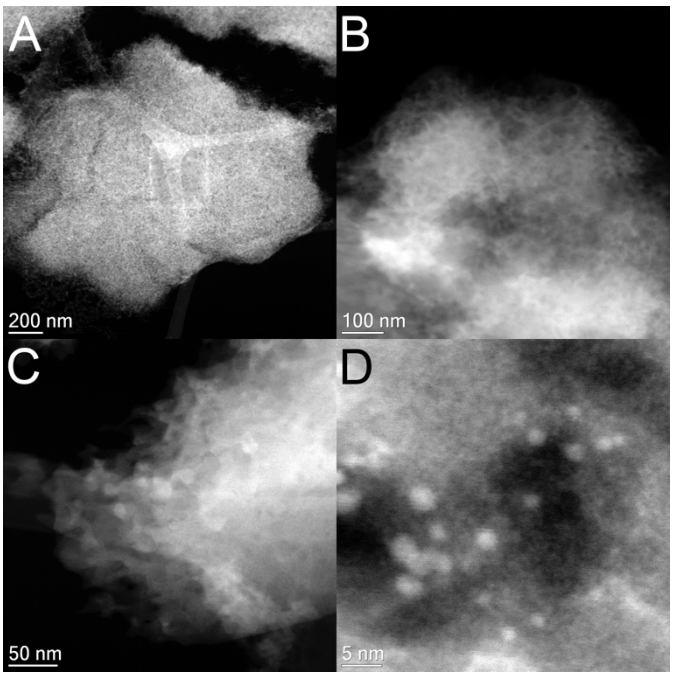

Figure 9 Cryo-STEM micrographs of the hydrometallogel of **2** (1:4 dilution in distilled water) at different microscopic augmentations. In (D), ultra-small Au NPs formed *in situ* could be observed.

of the dense cluttering of fine gold-containing fibers. This result is in stark contrast to the previously reported nanostructure of the other adeninegold(I) hydrogels (**Chart 1**), where straight nanofibers of micrometric length are observed, irrespective of self-assembly.

Quasi-elastic neutron scattering experiments

Finally, the dissimilar dynamical behaviour of the water molecules confined within the network of supramolecular fibers in **2** and **3** has been confirmed using the technique of quasi-elastic neutron scattering (QENS).[25] Experiments were performed on the near backscattering time-of-flight spectrometer IRIS at the ISIS Neutron and Muon Source (Didcot, United Kingdom) [26] which is used to probe molecular motions in the 10-100 ps range. The aim was to shed light (at least, partially) on the role of water in these systems, which is still obscure, despite being the major component of gold(I) hydrometallogels. We would expect that each gold(I) LMWG supramolecular assembly may distinctly affect in some way the swelling of water.

In a typical QENS experiment, the dynamical structure factor $S(Q,\omega)$ is obtained which is a function of wavevector transfer Q and the neutron-nucleus energy exchange ω, at a given temperature and pressure. $S(Q,\omega)$ is written as

$$S(Q,\omega) = R(Q,\omega) \otimes [\delta(\omega) + L(Q,\omega)] + BG \qquad (1)$$

where $\delta(\omega)$ and $L(Q,\omega)$ are the static (elastic) and dynamic (quasi-elastic) components, respectively, convoluted with the instrumental resolution $R(Q,\omega)$, and BG is an energy independent background contribution. For the hydrometallogel samples considered here, the main contribution to the total neutron scattering signal arises from the incoherent scattering

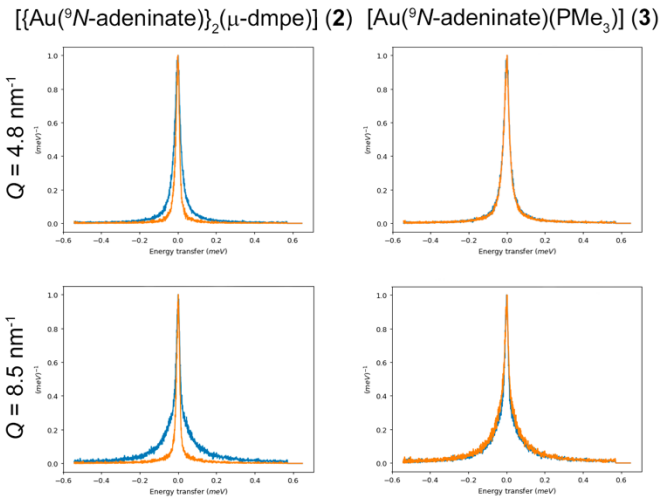

Figure 10 Superimposition of the normalized QENS profiles of the hydrometallogels of **2** and **3** (10% (w/w), orange curves) and neat water (blue curves), at T = 284 K and selected *Q* values.

of the hydrogen atoms of the water, since the pertaining cross-section, $\sigma_{inc}(^1H)$, is considerably larger than that of all other atoms in the compounds. This allows for a qualitative comparison of the diffusional freedom of water molecules in both situations, since the scattering contribution of the metallic complexes could be considered as residual.

The normalized QENS profiles of the hydrometallogels of **2** and **3** (10% w/w), superimposed with those of neat water, are plotted in **Figure 10**, for T = 284 K and at different values of *Q*. A simple inspection of **Figure 10** reveals that the scattering profile of **2** is clearly different to that of neat water for the considered *Q* values: more precisely, the quasi-elastic contribution (it is, the peak's basis broadening) in the former is much less evident than in the latter. Thanks to van Hove's deductions,[27] a direct relationship between quasi-elastic broadening and molecular self-motion can be established. Thus, water within the hydrometallogel of **2** is notably less mobile and thus highly restricted than in its pure form, a result that seems logical considering the solid-like nature of gels and the "spongey" aspect noticed in the cryo-STEM micrographs. However, the picture regarding **3** is, surprisingly, the opposite, as the profiles are fully overlapping. This would suggest that [Au(9*N*-adeninate)(PMe_3)] molecules and water ones interact in such a manner that the latter behave as in its pure form. These two contradicting results may be concealed if the mesoscopic structures of the hydrometallogels of **2** and **3** are recalled. Whereas that of **2** is dense, entangled and seemingly anarchic, the sequential self-assembly of **3** leads to the growing of parallel arrays of Ultra-thin NanoWires (UNWs).[15] The voids between the UNWs are expected to be filled with water molecules that, as QENS reveals, would be able to free-flow like pure water.

Conclusions

The preparation of a formal dimer of the well-established [Au(9*N*-adeninate)(PMe_3)] LMWG by the support of an aurophilic interaction with a suitable α,ω-diphosphine ligand gives rise to the blue-phosphorescent [{Au(9*N*-adeninate)}$_2$(μ-dmpe)], which still retains the hydrogelating behaviour of the parent compound. However, that apparently simple chemical modification has a dramatic impact in the mesoscale structure, mechanical strength and water swelling behaviour of the new gel, as demonstrated in here. A possible explanation for such differences may be found in the increased conformational freedom that the flexible α,ω-diphosphine bridge confers to the whole [{Au(9*N*-adeninate)}$_2$(μ-dmpe)] molecule. Being the two potentially hydrogelating subunits of complex **2** (they are, the analogues of complex **3**) always kept bound by strong, irreversible chemical bonds, they can rotate them as convenient without disrupting its "dimeric" nature but, consequently, preventing a better-defined higher supramolecular order that, for instance, gives rise to the UNWs of **3**. This suggests us that a structure-to-properties relationship applies in here, which should be considered for the future design of new gold(I) LMWGs. Further efforts will be devoted to the production of new examples of gold(I) LMWGs based on the adenine moiety and the rationalisation of the subtle factors affecting gelation.

Conflicts of interest

There are no conflicts to declare.

Acknowledgements

We gratefully acknowledge the DGI MICINN/FEDER (project number PID2019-104379RB-C22 (AEI/FEDER, UE)) and MCIU/FEDER (project number ECQ2018-004082 (AEI/FEDER, UE)) for financial support, and Laboratorio de Microscopías Avanzadas, Instituto de Nanociencia de Aragón for cryo-STEM facilities. D. Blasco acknowledges MIU (former MECD) for the concession of a FPU grant. J.A. Martínez-González acknowledges funding from the European Union's Horizon 2020 research and innovation programme under the Marie Skłodowska-Curie grant agreement Nº 665593 awarded to the Science and Technology Facilities Council. Neutron beamtime was awarded and data can be found in https://doi.org/10.5286/ISIS.E.RB1920572.

Notes and references

1 A. Y.-Y. Tam and V. W.-W. Yam, Recent advances in metallogels, *Chem. Soc. Rev.*, 2013, **42**, 1540-1567 (and references therein).
2 J. C. Lima and L. Rodríguez, Supramolecular gold metallogelators: the key role of metallophilic interactions, *Inorganics*, 2015, **3**, 1-18 (and references therein).
3 J. Chen, Z. Zhang, C. Wang, Z. Gao, Z. Gao and F. Wang, Cooperative self-assembly and gelation of organogold(I) complexes *via* hydrogen bonding and aurophilic Au···Au interactions, *Chem. Commun.*, 2017, **53**, 11552-11555.
4 N. Mirzadeh, S. H. Privér, A. J. Blake, H. Schmidbaur and S. K. Bhargava, Innovative molecular design strategies in materials science following the aurophilicity concept, *Chem. Rev.*, 2020, **120**, 7551-7591.
5 (*a*) H. Schmidbaur and A. Schier, A briefing on aurophilicity, *Chem. Soc. Rev.*, 2008, **37**, 1931-1951. (*b*) H. Schmidbaur and

A. Schier, Aurophilic interactions as a subject of current research: an up-date, *Chem. Soc. Rev.*, 2012, **41**, 370-412.
6 E. R. Draper and D. J. Adams, Low-molecular-weight gels: the state of the art, *Chem*, 2017, **3**, 390-410.
7 A. Codina, E. J. Fernández, P. G. Jones, A. Laguna, J. M. López-de-Luzuriaga, M. Monge, M. E. Olmos, J. Pérez and M. A. Rodríguez, Do aurophilic interactions compete against hydrogen bonds? Experimental evidence and rationalization based on *ab initio* calculations, *J. Am. Chem. Soc.*, 2002, **124**, 6781-6786.
8 J. M. Forward, J. P. Fackler, Jr. and Z. Assefa, in *Optoelectronic properties of inorganic compounds*, ed. J. P. Fackler, Jr., Plenum Press, 1999, Ch. 6, pp. 195-229.
9 W.-F. Fu, K.-C. Chan, K.-K. Cheung and C.-M. Che, Substrate-binding reactions of the ^{3}[dσ*pσ] excited state of binuclear gold(I) complexes with bridging bis(dicyclohexylphosphino)methane ligands: emission and time-resolved absorption spectroscopic studies, *Chem. Eur. J.*, 2001, **7**, 4656-4664.
10 H. Schmidbaur and H. G. Raubenheimer, Excimer and exciplex formation in gold(I) complexes preconditioned by aurophilic interactions, *Angew. Chem. Int. Ed.*, 2020, **59**, 14748-14771.
11 C. Jobbágy, P. Baranyai, G. Marsi, B. Rácz, L. Li, P. Naumov and A. Deák, Novel gold(I) diphosphine-based dimers with aurophilicity triggered multistimuli light-emitting properties, *J. Mater. Chem. C*, 2016, **4**, 10253-10264.
12 R. Hofmann and H. R. Schmidt, The isolobal analogy, *Angew. Chem. Int. Ed. Engl.*, 1986, **25**, 837-839.
13 H. G. Raubenheimer and H. Schmidbaur, Gold chemistry guided by the isolobality concept, *Organometallics*, 2012, **31**, 2507-2522.
14 (*a*) H. Schmidbaur, H. G. Raubenheimer and L. Dobrzańska, The gold-hydrogen bond, Au-H, and the hydrogen bond to gold, Au···H-X, *Chem. Soc. Rev.*, 2014, **43**, 345-380. (*b*) M. Rigoulet, S. Massou, E. D. S. Carrizo, S. Mallet-Ladeira, A. Amgoune, K. Miqueu and D. Bourissou, Evidence for genuine hydrogen bonding in gold(I) complexes, *Proc. Nat. Acad. Sci.*, 2019, **116**, 46-51. (*c*) M. Straka, E. Andris, J. Vícha, A. Růžička, J. Roithová and L. Rulíšek, Spectroscopic and computational evidence of intramolecular Au^{I}···H^{+}-N hydrogen bonding, *Angew. Chem. Int. Ed.*, 2019, **58**, 2011-2016. (*d*) H. Schmidbaur, Proof of concept for hydrogen bonding to gold, Au···H-X, *Angew. Chem. Int. Ed.*, 2019, **58**, 5806-5809.
15 D. Blasco, J. M. López-de-Luzuriaga, M. Monge, M. E. Olmos, D. Pascual and M. Rodríguez-Castillo, Cooperative Au(I)···Au(I) interactions and hydrogen bonding as origin of a luminescent adeninate hydrogel formed by ultrathin molecular nanowires, *Inorg. Chem.*, 2018, **57**, 3805-3817.
16 D. Blasco, J. M. López-de-Luzuriaga, M. Monge, M. E. Olmos and M. Rodríguez-Castillo, Balancing ionic and H-bonding interactions for the formation of Au(I) hydrometallogels, *Dalton Trans.*, 2019, **48**, 7519-7526.
17 E. R. T. Tiekink, T. Kurucsev and B. F. Hoskins, X-ray structure and UV spectroscopic studies of (adeninato-*N*9)triethylphosphinegold(I), *J. Crystallogr. Spectroscop. Res.*, 1989, **19**, 823-838.
18 Y. Rosopulos, U. Nagel and W. Beck, Metallkomplexe mit biologisch wichtigen liganden, XXXIV. Allyl-palladium(II)- und triphenylphosphan-gold(I)-komplexe mit nucleobasen und nucleosiden, *Chem. Ber.*, 1985, **118**, 931-942.
19 D. Blasco, J. M. López-de-Luzuriaga, M. Monge, M. E. Olmos, D. Pascual and M. Rodríguez-Castillo, Time-dependent molecular rearrangement of [Au(*N*^{9}-adeninate)(PTA)] in aqueous solution and aggregation-induced emission in a hydrogel matrix, *Inorg. Chem.*, 2021, **60**, 3667-3676.
20 U. E. I. Horvath, S. Cronje, J. M. McKenzie, L. J. Barbour and H. G. Raubenheimer, Mono- and binuclear gold(I) amido compounds of purine derivatives, *Z. Naturforsch B: J. Chem. Sci.*, 2004, **59**, 1605-1617.
21 H.-R. C. Jaw, M. M. Savas, R. D. Rogers and W. R. Mason, Crystal structures and solution electronic absorption and MCD spectra for perchlorate and halide salts of binuclear gold(I) complexes containing bridging $Me_2PCH_2PMe_2$ (dmpm) or $Me_2PCH_2CH_2PMe_2$ (dmpe) ligands, *Inorg. Chem.* 1989, **28**, 1028-1037.
22 S. S. Batsanov, Van der Waals radii of elements, *Inorg. Mater.*, 2001, **37**, 871-885.
23 K. Araki and I. Yoshikawa, Nucleobase-containing gelators, *Top. Curr. Chem.*, 2005, **256**, 133-165.
24 G. M. Peters and J. T. Davis, Supramolecular gels made from nucleobase, nucleoside and nucleotide analogs, *Chem. Soc. Rev.*, 2016, **45**, 3188-3206.
25 (*a*) J. S. Gardner, G. Ehlers, A. Faraone and V. García Sakai, High-resolution neutron spectroscopy using backscattering and neutron spin-echo spectrometers in soft and hard condensed matter, *Nat. Rev. Phys.*, 2020, **2**, 103-116. (*b*) V. García Sakai and A. Arbe, Quasielastic neutron scattering in soft matter, *Curr. Opin. Colloid Interface Sci.*, 2009, **14**, 381-390.
26 ISIS Neutron and Muon Source, IRIS homepage https://www.isis.stfc.ac.uk/Pages/iris.aspx.
27 L. van Hove, Correlations in space and time and Born approximation scattering in systems of interacting particles, *Phys. Rev.*, 1954, **95**, 249-262.

